A Methodology for the Reverse Engineering of the Energy Management Strategy of a Plug -In Hybrid Electric Vehicle for Virtual Test Rig Development

ARTICLE INFO
Article ID: 14-11-01-0009

doi:10.4271/14-11-01-0009

A Methodology for the Reverse Engineering of the Energy Management Strategy of a Plug-In Hybrid Electric Vehicle for Virtual Test Rig Development

Federico Millo,[1] Luciano Rolando,[1] Luca Pulvirenti,[1] and Giuseppe Di Pierro[1]

[1]Politecnico di Torino, Italy

Abstract

Nowadays, the need for more sustainable mobility is fostering powertrain electrification as a way of reducing the carbon footprint of conventional vehicles. On the other side, the presence of multiple energy sources significantly increases the powertrain complexity and requires the development of a suitable Energy Management System (EMS) whose performance can strongly affect the fuel economy potential of the vehicle. In such a framework, this article proposes a novel methodology to reverse engineer the control strategy of a test case P2 Plug-in Hybrid Electric Vehicle (PHEV) through the analysis of experimental data acquired in a wide range of driving conditions. In particular, a combination of data obtained from On-Board Diagnostic system (OBD), Controller Area Network (CAN)-bus protocol, and additional sensors installed on the High Voltage (HV) electric net of the vehicle is used to point out any dependency of the EMS decisions on the powertrain main operating variables. Furthermore, the impact that Vehicle-to-Infrastructure (V2I) connections have on the control law is assessed on several tests performing the same real-world route with the vehicle navigation system alternatively switched on and off. Finally, a virtual test rig of the tested vehicle, developed in the GT- SUITE environment, is used to validate the set of extracted rules against the experimental data. An error of about 1-2% on the prediction of the vehicle CO_2 emissions and good matching of the State of Charge (SoC) profile in both Charge Depleting (CD) and Charge Sustaining (CS) phases prove the effectiveness of the proposed methodology.

History

Received: 30 Mar 2021
Revised: 03 Jul 2021
Accepted: 01 Sep 2021
e-Available: 22 Sep 2021

Keywords

Reverse engineering, Energy management system, Hybrid electric vehicle, Real driving conditions

Citation

Millo, F., Rolando, L., Pulvirenti, L., and Di Pierro, G., "A Methodology for the Reverse Engineering of the Energy Management Strategy of a Plug-In Hybrid Electric Vehicle for Virtual Test Rig Development," *SAE Int. J. Elect. Veh.* 11(1):2022, doi:10.4271/14-11-01-0009.

ISSN: 2691-3747
e-ISSN: 2691-3755

1. Introduction

In the last decades, environmental awareness has increased dramatically, and the risks connected to climate change have fostered the introduction of challenging targets to limit the growth of Greenhouse Gases (GHGs) emissions [1, 2]. At the 2015 United Nations Climate Change Conference (COP21), one of the foremost global climate deals was adopted: it was aimed at "limiting global warming to well below 2°C" compared to pre-industrial levels [3]. However, bucking the trend of other sectors, the CO_2 emissions generated by the transport sector have increased between 1990 and 2016 [4]. In 2017, it was responsible for 27% of the total European Union (EU-28) GHGs emissions. Indeed, road transport was responsible for almost 72% of total GHGs from transport [5]. To curb this trend, the EU has tightened its CO_2 emissions targets for the upcoming years, requiring, for newly registered passenger cars, a 15% and a 37.5% reduction in 2025 and 2030, respectively, in comparison to the 2021 levels [6, 7].

In this framework, among the feasible technical solutions improving the efficiency of current propulsion systems, Hybrid Electric Vehicles (HEVs) and Plug-in Hybrid Electric Vehicles (PHEVs) have received lots of attention thanks to their potentialities to reduce fuel consumption within realistic economical, infrastructural, and customer acceptance constraints [8, 9]. In a hybrid powertrain, an Internal Combustion Engine (ICE) is combined with one or more Electric Machines (EMs) and with a High Voltage (HV) battery pack [10]. Nevertheless, despite its potential, powertrain electrification introduces complexity and degrees of freedom due to the coexistence and cooperation of more power actuators. Therefore, the benefits provided by hybridization can be fully exploited only by means of an ad hoc powertrain control strategy [11]: a high-level controller, namely, the Energy Management System (EMS), must be added to optimize the energy flow on the vehicle [12, 13].

In the literature, different categories of strategies have been proposed. However, the exponential growth of computational capabilities and the introduction of new technologies, such as Vehicle-to-Everything (V2X) connectivity, will expand both the potential and the complexity of the energy management of HEVs [14]. Within this variety, a general classification can be outlined identifying two general trends: rule-based and model-based optimization methods [15]. Among the model-based methods, the global optimization ones, e.g., Dynamic Programing [16, 17], implement a control law to find a globally optimal solution. Nevertheless, they require computational time incompatible with real-time execution, and they must be provided with a priori information regarding the mission profile. On the contrary, the local optimization methods, e.g., Equivalent Consumption Minimization Strategy (ECMS) [18, 19] or Pontryagin's Minimum Principle [20], implement instant-wise control decisions aimed at the instantaneous minimization of the fuel consumption. Despite their feasibility in a physical dynamic system, their results are necessarily suboptimal. On the other hand, thanks to their notably limited computational effort, the most common implementation of an HEV supervisory control relies on heuristic control techniques: a set of rules that, on the base of some meaningful observed variables, decides the power split among the on-board power sources [21].

In this context, it is of paramount importance to assess the state-of-the-art energy management strategies already existing in the market. On the contrary, given the novelty of hybrid powertrains and their intrinsic complexities, carmakers are very jealous of this technical know-how, and they do not easily make disclosures about their techniques. Finally, investigating the EMS of a vehicle already available in the market is extremely demanding because it requires a significant amount of experimental data and a reliable methodology in the extraction of information from a complex system such as a vehicle Electronic Control Unit (ECU) [22].

Only a few researchers have addressed the problem of reverse engineering the strategy, followed by a real EMS. In [23], the French National Institute for Transport and Safety Research (INRETS) tested the 2004 Toyota Prius: a coupled approach was performed, associating simulations with experimental validation. At the Argonne National Laboratory, an HEV—the 2010 Toyota Prius—and an Extended-Range Electric Vehicle, the 2014 BMW i3, were tested. In both cases, a vehicle model was built and validated with the results of the testing [24, 25]. In [26] a parallel PHEV was tested, and the experimental results were investigated in order to extract the control logic of the EMS without direct access to it. In [27] a PHEV, along with two conventional vehicles, was studied by collecting experimental data to assess its real-world CO_2 emission under different conditions and to develop a generic vehicle simulation model. Nevertheless, a more generalized approach for extracting the strategy implemented in an EMS has not yet been proposed.

In this framework, this article focuses on an innovative methodology for reverse engineering the strategy implemented in the EMS of a hybrid powertrain. In this work, the experimental results of [28], where DiPierro et al. tested a Euro 6d-temp P2 diesel PHEV available in the European market, were carefully analyzed and post-processed in order to extract the strategy adopted by the EMS, pointing out any dependency of its decisions on the powertrain's main operating variables. The purpose of this study is to build a virtual test rig for a commercially available PHEV without having direct access to its EMS, but only exploiting, through reverse engineering, the information gathered from an extensive experimental campaign.

The accuracy of the extracted strategy and the effectiveness of the proposed methodology was assessed through numerical simulation, by modelling the vehicle in GT-SUITE, coupled to the extracted EMS developed in Simulink®. The good matching between the simulation results and the experimental data confirmed the robustness of the methodology for reverse engineering the strategy implemented in a real EMS.

This article is organized as follows: after presenting the main features of the case study (Section 2), the article describes the developed methodology for reverse engineering the strategy implemented in the EMS (Section 3).

Then the modelling approach is presented (Section 3.5) along with the model validation (Section 3.6). Finally, the results obtained in a Real Driving Emissions (RDE) simulation are shown (Section 4).

2. Case Study

The vehicle under investigation is the Mercedes E300de, a state-of-the-art diesel PHEV available in the European market. It features a P2 architecture, and the powertrain layout is schematically shown in Figure 1. A Euro 6d-temp 1950 cc diesel engine, fitted at the front of the vehicle in a longitudinal position, is integrated and connected, through an auxiliary clutch (K0), to an EM of Permanent Magnet (PM) synchronous type. Both the ICE and the EM are connected, through a Torque Converter and a nine-speed Automatic Transmission (AT), to the rear axle. The EM is powered by a 13.5 kWh Li-Ion Nickel-Manganese-Cobalt-oxide (Li-NMC) HV battery. A DC/DC converter allows the HV battery to feed the 12 V battery and all the Low Voltage (LV) loads (i.e., the 12 V starter and the electrical oil pump for gearbox lubrication). The main vehicle characteristics are summarized in Table 1.

Typically, PHEVs can operate in two different modes:

- **Charge Depleting (CD):** when the battery is fully or partially charged, the vehicle is mainly propelled in fully electric mode.
- **Charge Sustaining (CS):** when the battery State of Charge (SoC) reaches a certain minimum threshold defined in calibration, the ICE is used for propulsion and the SoC is maintained within a small window.

TABLE 1 Vehicle and powertrain main specifications.

Vehicle			
Cycle	**NEDC**	**WLTC**	
Test Mass*	2040 kg	2162 kg	
F0*	152.9 N	171.5 N	
F1*	0.809 N/km/h	0.833 N/km/h	
F2*	0.0272 N/(km/h)^2	0.0280 N/(km/h)^2	
Configuration	Rear wheel drive (RWD)		
Transmission			
Type	9-AT w/ torque converter		
Speed ratios	I 5.36	IV 1.64	VII 0.87
	II 3.25	V 1.22	VIII 0.72
	III 2.26	VI 1.00	IX 0.61
Reverse	−4.93	Final drive	2.65
Engine (ICE)			
Engine type	In-line 4 cylinders turbo diesel		
Displacement	1950 cm^3		
Max power/Max torque	143 kW at 3800 rpm/400 Nm at 1600-2800 rpm		
Compression ratio	15.5:1		
Electric Machine (EM)			
Type	PM synchronous motor		
Max power/Max torque	90 kW at 2000 rpm/440 Nm at 1750 rpm		
Max speed	6000 rpm		
High voltage battery			
Type	Li-NMC		
Rated voltage	365 V		
Capacity	13.5 kWh/37 Ah		
Cooling system	Water cooled		

* Please note that test procedures require different masses and coastdown coefficients for NEDC and WLTP.

FIGURE 1 Powertrain layout with instrumentation details: It features a P2 architecture in which a diesel engine is connected through an auxiliary clutch to an EM. Both the ICE and the EM are connected to the AT by means of a torque converter. The layout is an RWD one.

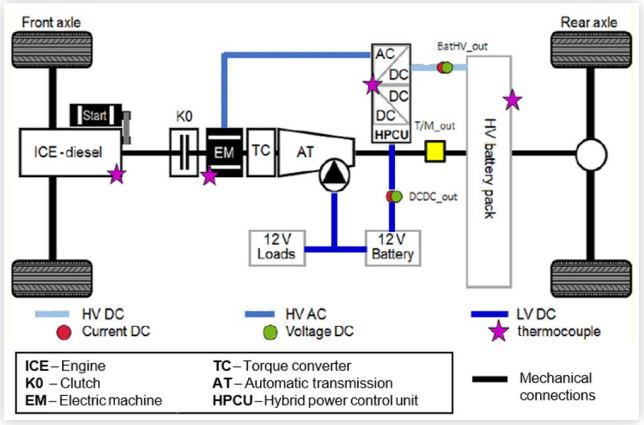

In the investigated vehicle, a Hybrid Power Control Unit (HPCU) is connected to the HV inverter, which handles the energy flows between the EM and the HV battery pack. The HPCU allows the driver to select between four different driving modes:

- **Hybrid Drive:** it is the default setting; the EMS autonomously decides the powertrain operating mode depending on the driving situation and the route profile.
- **Electric Drive:** this setting ensures zero local emissions because it is performed in CD mode; the power necessary to propel the vehicle is provided by the E-motor.
- **E-Save Drive:** this mode ensures the CS of the battery SoC, in order to allow the electric drive at a later stage; thus, the E-motor propels the vehicle in combination with the ICE.
- **Charge Drive:** this mode ensures that only the ICE propels the vehicle, while constantly charging the battery.

It is worth mentioning that during the test campaign, the hybrid drive was always selected so that the EMS autonomously decided the energy management of the hybrid powertrain.

Most of the experimental campaign was carried out on an All-Wheel Drive (AWD) chassis dynamometer, but some additional measurements (the RDE tests shown in Table 2) were performed in real-world scenarios, equipping the vehicle with a Portable Emissions Measurement System (PEMS). In particular, the HORIBA OBS One PEMS device was used. The powertrain was fully characterized without performing an expensive complete teardown: only the ICE was characterized in terms of Brake-Specific Fuel Consumption (BSFC) maps, as described in [28]. A combination of data was obtained from Controller Area Network (CAN)—bus protocol, On-Board Diagnostic (OBD) system, and additional sensors installed in strategic locations. In Figure 1 the instrumentation details are shown on the powertrain layout: the EM inverter and the DC/DC LV side were electrically instrumented with a high precision current and voltage measurement system. Because of the system complexity and the huge effort required in the data acquisition and processing, the EM was not instrumented: its characterization was carried out combining the measurement of the electrical energy on the DC side with data available from the CAN—bus protocol. In fact, the EM torque and rotational speed, as well as the ICE ones, were acquired from CAN. Finally, the magenta stars in Figure 1 represent the temperature sensors, placed in: the inlet/outlet of the ICE cooling circuit, the inlet/outlet of the HV battery cooling system, the HV battery pack surface, the inlet/outlet of the HPCU, and the EM surface.

The characteristic values of the performed cycles are shown in Table 2. As far as regulatory driving cycles (i.e., NEDC and WLTC) are concerned, measurements were performed on the chassis dynamometer following the Type-Approval (TA) procedure [29]. For a PHEV, the guidelines defined in the UNECE Regulation 83 require two tests in different conditions [30]:

1. Condition A: the HV battery must be fully charged at the beginning of the test.
2. Condition B: the HV battery must be at minimum SoC at the beginning of the test.

Hereinafter, Condition A will be indicated as CD phase, while Condition B as CS phase.

The RDE cycles, which were performed to fully characterize the powertrain control logic, were conducted on the public roads in the surroundings of the Italian city of Turin. RDE_1 and RDE_2 were specific tests aimed at assessing the reliance of the EMS decisions on the Global Positioning System (GPS) information: they feature the same real-world route with the vehicle navigation system alternatively switched on and off. RDE_3, instead, was conducted under a predefined RDE compliant route [31], which is illustrated in Figure 2. In Figure 3, the vehicle speed and altitude profiles of the RDE_3 are plotted against the travelled distance. A rural and a motorway operation follow the urban one, involving both uphills and downhills. The total test lasted approximately 92 minutes and covered a distance of around 96 km.

3. Methodology

As outlined in the introduction, the aim of the work is to develop a methodology to analyze the behavior of the strategy followed by the EMS. The proposed methodology tries to identify the control logic without direct access to the EMS and a detailed characterization of ICE, EM, and HV battery. The data acquired during the experimental campaign was arranged in some specific plots to point out the dependency of the EMS decisions on the main powertrain operating variables. As an example, in Figure 4 the typical layout of the NEDC vehicle speed profile in the function of time is displayed. Two different operating modes are considered:

- **EV Mode**: the EM delivers all the required torque (green points).
- **Parallel Mode**: both the ICE and the EM deliver the required torque (blue points).

The parameter chosen for discriminating the two modes is the engagement of the clutch K0 (see Figure 1), between ICE and EM. As a matter of fact, in the Electric Vehicle (EV) mode, the clutch is disengaged, and the ICE is off while, in the parallel mode, the clutch is engaged and the ICE is coupled to the EM and the transmission. It should be noted that the abovementioned classification is just a preliminary differentiation between the operating conditions, while further details about power split, load point moving, e-assist, etc. will be discussed in the following paragraphs.

For the sake of brevity, only the WLTC results will be presented in the following section, although several other cycles were used in the overall analysis. As it can be seen from Figure 5(a), the cycle is repeated several times according to

TABLE 2 Characteristic values of the cycles performed to characterize the powertrain control logic.

Cycle Unit	Time [s]	Distance [km]	Avg. speed [km/h]	Max speed [km/h]	Avg. acc. [m/s²]	Max acc. [m/s²]	Required energy [Wh/km]
NEDC	1180	11	34	120	0.38	1.42	184
WLTC	1800	23	47	131	0.41	1.84	222
RDE_1	4327	68	57	144	0.37	1.91	273
RDE_2	4322	68	57	128	0.36	1.74	258
RDE_3	5532	96	63	138	0.35	4.22	223

FIGURE 2 RDE_3 route definition: vehicle position obtained from PEMS and combined with topographic map (Courtesy of Google Maps). Urban, rural, and motorway sections are defined according to the Regulation [33] and are depicted respectively in orange, green, and blue.

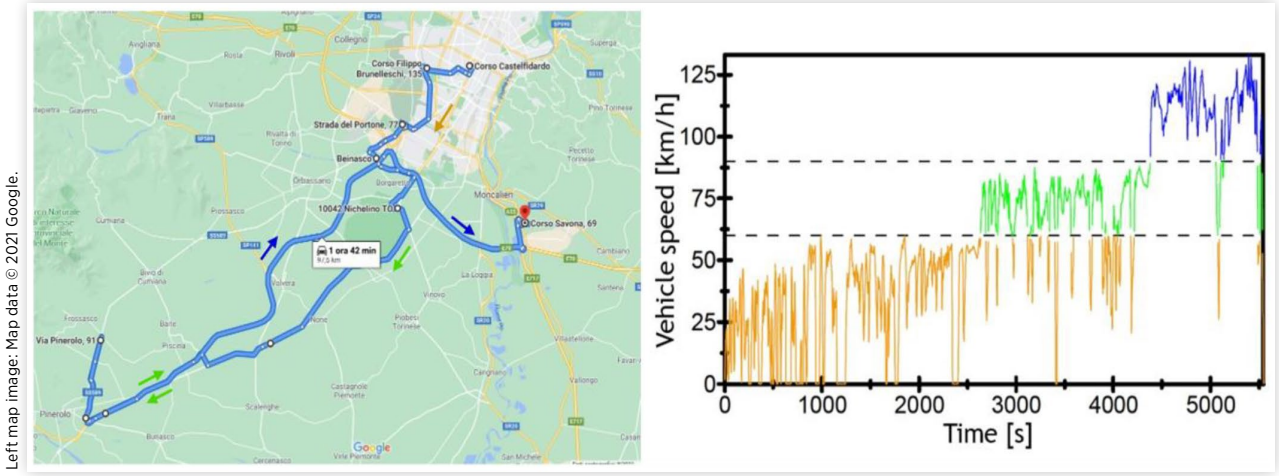

FIGURE 3 RDE_3 speed/altitude profile in the function of the travelled distance. The vehicle mission lasted approximately 92 minutes and covered a distance of around 96 km with an altitude variation of about 120 m.

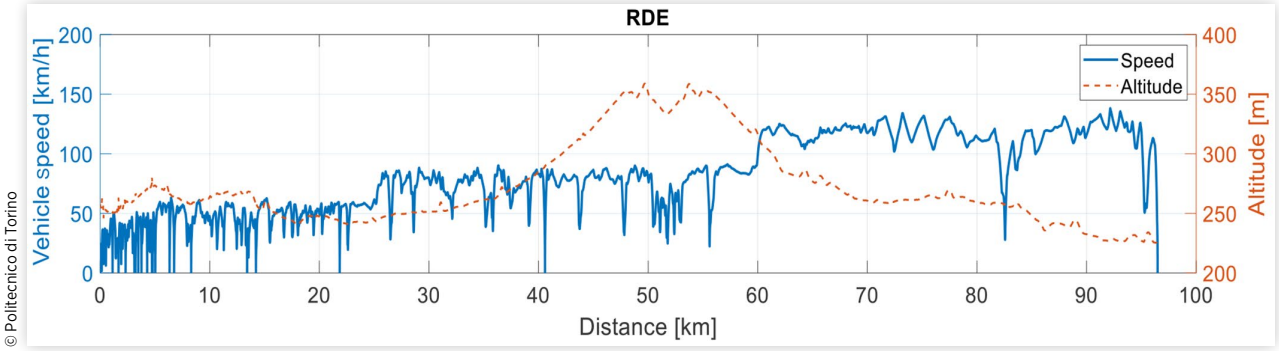

FIGURE 4 Vehicle tested over the NEDC. (a) Vehicle speed profile along with the operating modes: EV mode (green) and parallel mode (blue); (b) Engine state: 1 (on) and 0 (off).

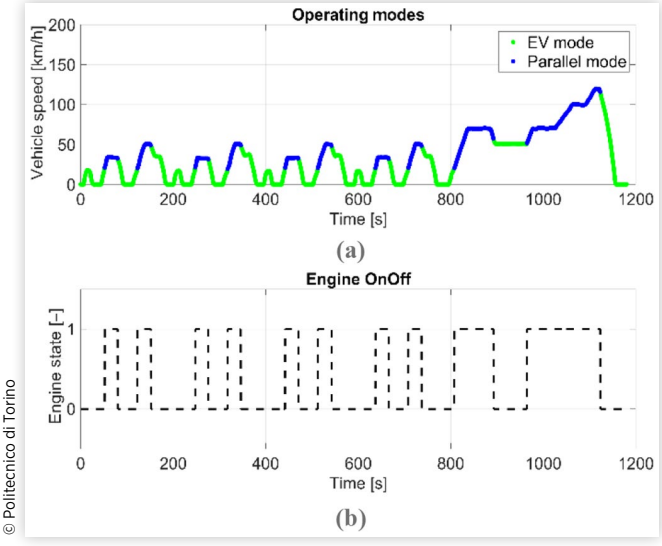

FIGURE 5 WLTC repetitions according to the Regulation [30]. (a) Vehicle speed profile along with the operating modes: EV mode (green) and parallel mode (blue). (b) Battery SoC profile in the function of time. The dashed area highlights the section performed in CD mode.

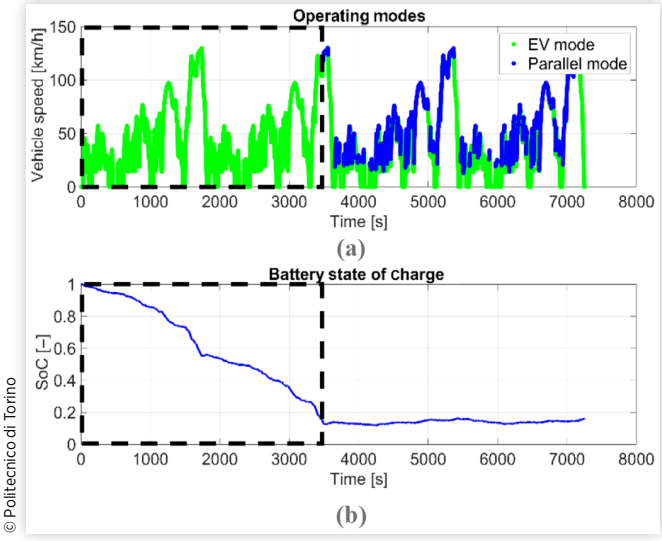

TABLE 3 Different variables measured at the instant of a switch from CD to CS operation in all the considered mission profiles.

Cycle Unit	Time [s]	Distance [km]	SoC_{min1} [—]
NEDC	5788	51.1	0.13
WLTC	3488	43.2	0.13
RDE_1	2301	41.9	0.13
RDE_2	—	—	—
RDE_3	3210	37.2	0.13

the Regulation [30]. The vehicle performs twice the WLTC in CD mode (marked with a dashed area), and the ICE is switched on only at the end of the second cycle. Furthermore, Figure 5(b) highlights that the CS mode is enabled only when the electrical storage device reaches low values of the SoC. From the analysis of the SoC trajectory over the different driving cycles, a switching threshold of about 13% could be identified (see Table 3). For the cycle, RDE_2 data are not available because the CS phase is never reached (see Section 3.4).

In the subsequent sections, the vehicle behavior, during both CD and CS phases, will be analyzed more in detail.

3.1. Rules in CD

As already mentioned, the analysis of the black box (represented in Figures 5 and 6) points out that all the CD phase is carried out in fully electric mode: the ICE is never switched on and the EM alone delivers all the required power.

Different behavior can be noticed in the RDE_1 test (represented in Figure 7): the ICE is switched on (red dots) also during the CD phase when higher loads are required. Indeed, analyzing the EM operating points, reported in Figure 8, it is eye-catching that, during the CD phase, the ICE is usually switched on (red dots) when the EM reaches its max performance. Moreover, it can be observed that in parallel mode the EM spends most of the time at very low loads, implying the vehicle is operating in a pure ICE drive. All the gray dots represent the transition phases during which the engine status and the clutch engagement are changing.

FIGURE 6 Power delivered by the actuators during the WLTC repetitions according to the Regulation [30]. (a) ICE; (b) EM.

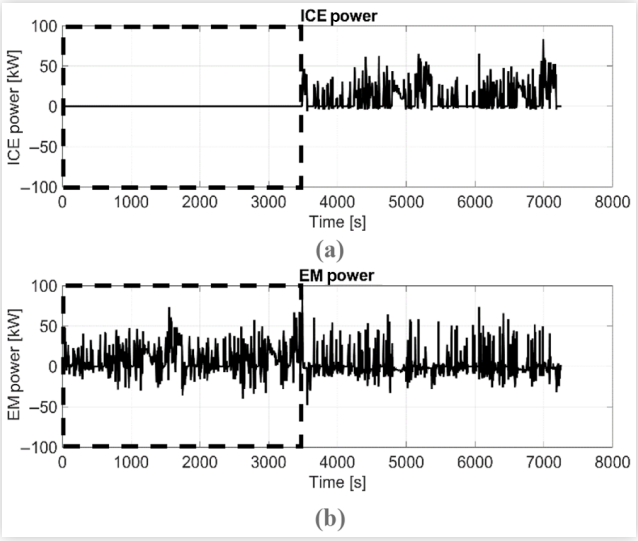

FIGURE 7 RDE_1. (a) Vehicle speed profile along with the operating modes: EV mode (green) and parallel mode (blue); (b) Battery SoC profile in the function of time. The dashed area highlights the section performed in CD mode. The ICE switching on during the CD phase is denoted with red dots.

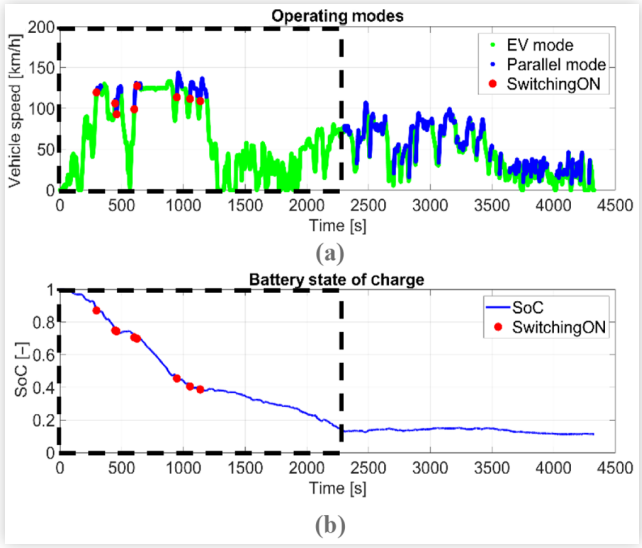

FIGURE 8 RDE_1—EM working points in speed (x-axis) power (y-axis) map and full-load curve. Green dots: EV mode; blue dots: parallel mode; red dots: engine switching on; gray dots: transition phases, i.e., the engine status and the clutch engagement are changing.

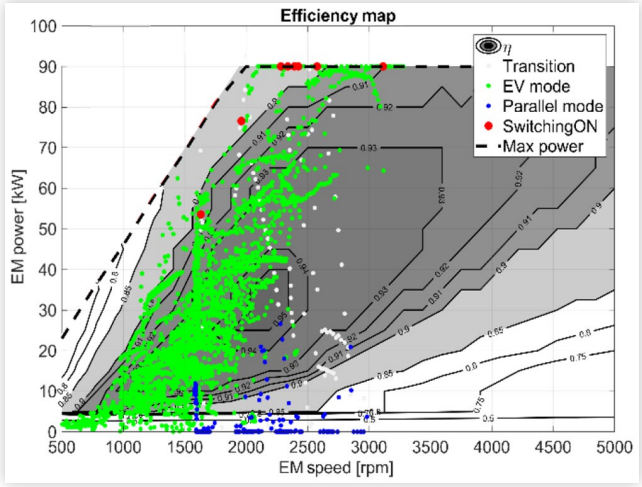

FIGURE 9 RDE$_1$—EM power represented in the function of the total powertrain power. Green dots: EV mode; blue dots: parallel mode; gray dots: transition phases, i.e., the engine status and the clutch engagement are changing.

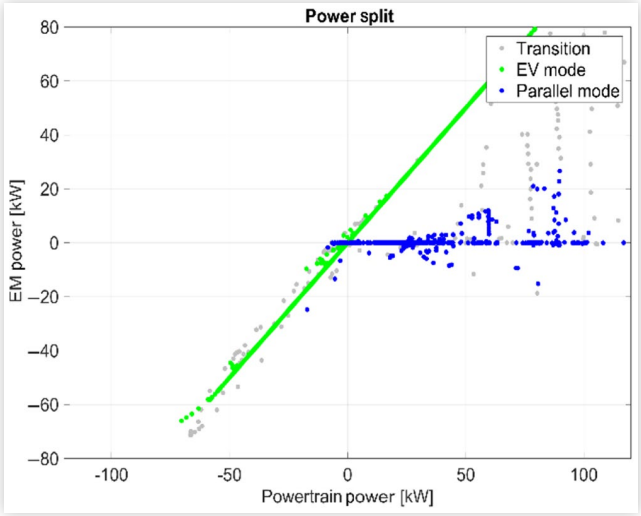

The same behavior can be more clearly observed in Figure 9, where the EM power is represented depending on the total powertrain power. The driver power request is almost totally fulfilled by the EM and the ICE, in EV and parallel mode, respectively: as a matter of fact, most of the points lay on the bisector and the x-axis. As already mentioned, the gray dots represent transition paths from EV to parallel mode.

3.2. Rules in CS

Since in CS the energy must be ultimately provided by the ICE, it is essential to extrapolate the ICE control pattern for understanding the logic of the powertrain EMS; thus, a more detailed analysis of both the ICE switching strategy and power split was performed. In Figure 10, the engine switching on and off are depicted (red bullets and yellow squares, respectively) on the vehicle speed profile of a WLTC featuring an already warmed-up ICE.

The operating conditions corresponding to the engine switch on/off were collected in order to highlight any dependency of the engine control on them. Figure 11(a) shows all the engine ignition points during the WLTC, depending on the vehicle acceleration and the vehicle speed. As expected, the higher the acceleration required by the driver the lower the vehicle speed threshold for ICE switching on; by interpolating the mapped points with a hyperbola branch (depicted in red), a clear pattern can be identified. Similarly, Figure 11(b) shows all the engine shutdown points (always for the WLTC) as a function of powertrain torque and vehicle acceleration. In particular, the lower the torque required by the driver the higher the vehicle deceleration threshold for ICE switching off. This control rule seems reasonable for safety reasons: the opening of the clutch K0 is delayed during higher decelerations since the combinations of engine inertia, pumping, and

FIGURE 10 Engine switching on and off during a WLTC featuring an already warmed-up ICE.

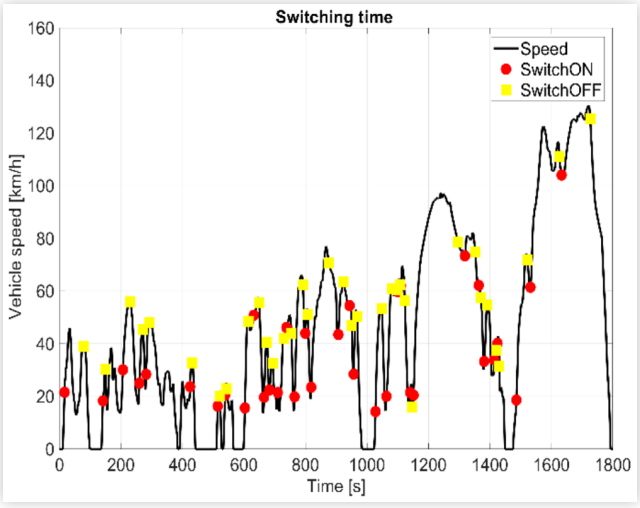

friction losses can provide additional braking power to the drivetrain. Moreover, a frequency limit on the change of the engine state was detected: the ICE must stay on for at least 5 s and off for at least 4 s.

Once the rules governing the ICE switching on and off had been extracted also for the CS phase, a more specific analysis was conducted to characterize the torque split in parallel mode. Firstly, the engine operating points were analyzed to investigate any predefined operating line followed by the engine, as found out for the Toyota 2010 Prius in [24].

FIGURE 11 Mapping of engine switching on and off during a WLTC featuring an already warmed-up ICE. (a) Engine switch-on points as a function of vehicle acceleration and speed; (b) Engine shutdown points as a function of powertrain torque and vehicle acceleration.

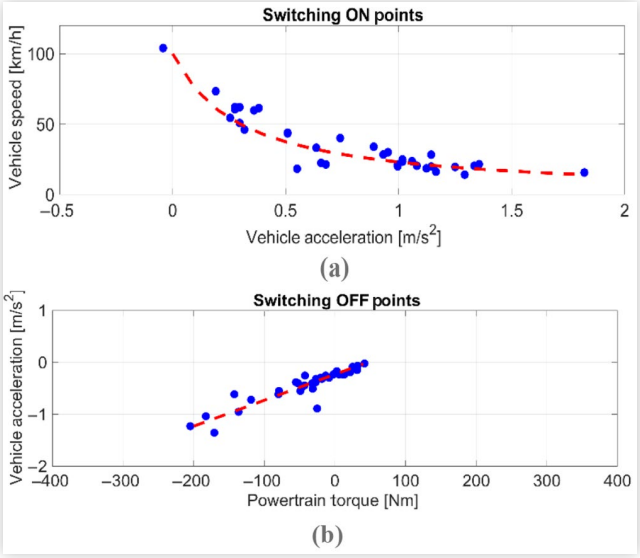

FIGURE 12 Engine operating points during a WLTC featuring an already warmed-up ICE.

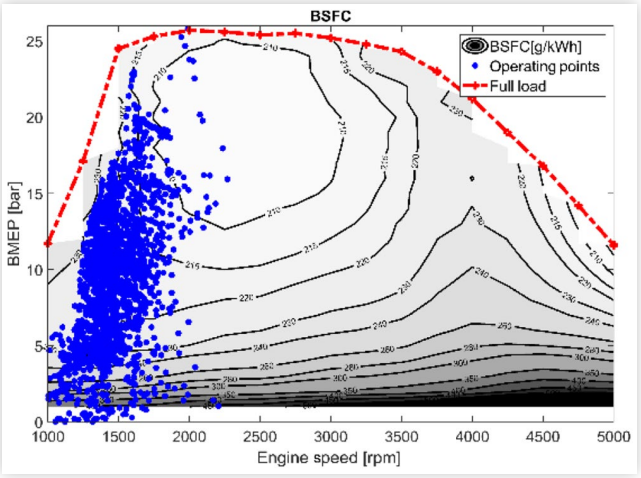

In Figure 12, where the operating points of the engine are represented on its BSFC map, no predefined pattern can be detected. The powertrain operating variables were therefore analyzed differently.

A clearer trend could be highlighted by investigating the torque split among the on-board power sources. In Figure 13 all the engine operating points during the WLTC are represented as a function of the total torque delivered by the powertrain and the torque delivered by the ICE. The points that lay on the red line ($P_{ICE} = P_{PWT}$) represent an ICE-only mode; under the red line, an e-boost is performed, while, above the red line, the powertrain operates in Load Point Moving (LPM)—i.e., the ICE operating points are shifted toward higher loads to allow battery recharging. As evident from Figure 13, for the analyzed cycle, an e-boost is almost never performed (the points under the bisector represent only transitional phases). On the contrary, the ICE always works in LPM, boosting the battery recharge. In particular, it can be noted that the lower the requested power the stronger the shift of the engine operating points toward higher loads, in order to counterbalance the BSFC worsening at low ICE loads.

FIGURE 13 WLTC—ICE torque represented in the function of the total powertrain torque. Blue dots: parallel mode; gray dots: transition phases, i.e., the engine status and the clutch engagement are changing.

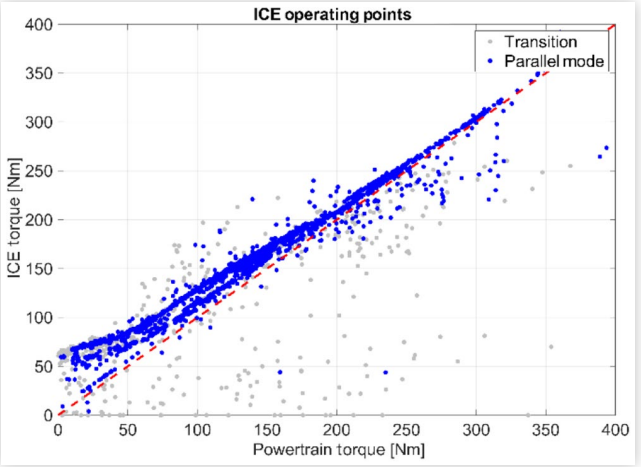

As previously mentioned, the "steady-state" operating modes have been highlighted since the gray points represent transition paths from EV to parallel mode. An almost linear relationship can be identified between the torque delivered by the ICE and the total torque delivered by the powertrain. However, the rule governing the torque split appeared to change according to the SoC trend. This behavior can be more clearly understood from Figure 14, where the WLTC has been subdivided into different time intervals (a, b, c, d) depending on the SoC values. For each subsection, the upper plot displays both SoC and speed profiles versus time, while the lower plot shows the corresponding torque split law. Depending on SoC values, different relationships between the ICE and the total torque can be highlighted. Apart from the first section—Figure 14(a)—where a different behavior is evident due to engine warm-up, if the SoC is above a certain threshold, Figures 14(b) and (d), the torque delivered by the engine appears to be closer to the red line, where the total torque request is coincident with the ICE torque and thus corresponding to the ICE-only mode. As a consequence, the ICE power exceeding the traction request, which is available for battery recharging, is quite limited, and for this reason, this rule will hereafter be referred to as "weak rule." On the other hand, when the SoC is below the threshold—Figure 14(c)—the deviation from the red line, where the total torque request is coincident with the ICE torque, is more evident: as a consequence, a higher ICE power is available for battery recharging, and for this reason, this rule will hereafter be referred to as "strong rule". For the sake of clarity, Figure 15 shows an enlargement of the two rules governing the torque split (i.e., the abovementioned "weak" and "strong" rules), entailing a softer and stronger recharge of the battery, respectively. The evidence from all the analyzed cycles suggests that the defined complex behavior, governing the torque split in the CS phase, is aimed at guaranteeing the charge sustainability, trying to ensure an SoC swing in the range (13%-15%).

As well as guaranteeing the charge sustainability, the LPM allows the ICE to work at higher loads, which means higher efficiencies. To assess the impact of the powertrain control strategy on the overall engine efficiency, the analyzed cycle was compared, through numerical simulation, to the same vehicle operating in ICE-only mode. Figure 16 displays the energy delivered by the engine during the WLTC, where the operating points have been grouped in different load bars representing the ICE energy share with respect to its relative load percentage. It is eye-catching that during the hybrid drive (green bars), the energy is delivered by the engine with a significantly higher efficiency in comparison with the ICE-only mode (blue bars).

FIGURE 14 WLTC subdivision in different time intervals (a, b, c, d) depending on the SoC values. Upper plot: SoC and speed profiles vs time; Lower plot: correspondent torque split law.

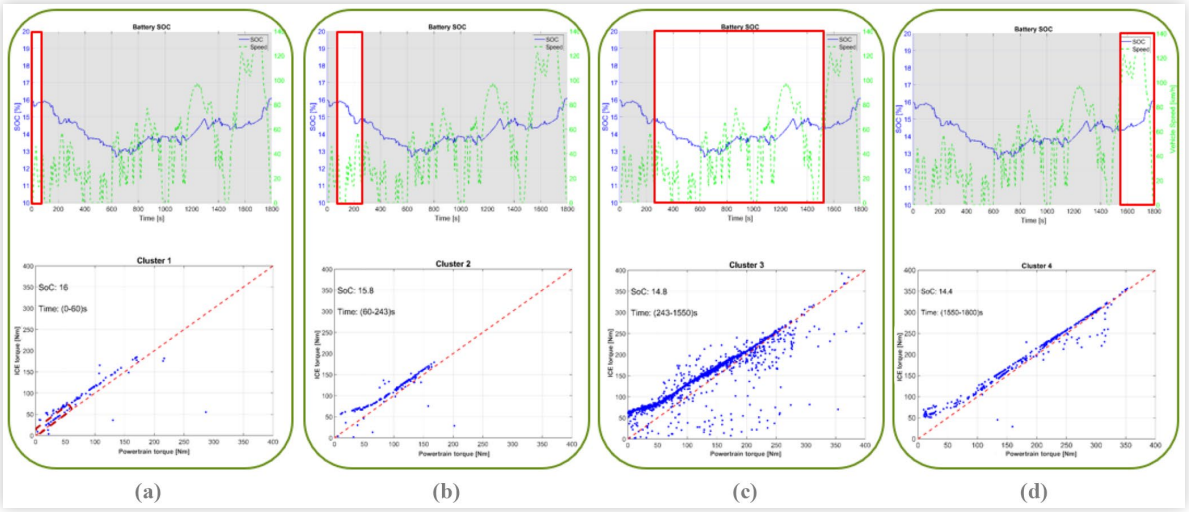

FIGURE 15 Extraction of the rules governing the torque split. (a) "Weak rule" entailing softer recharge of the battery; (b) "Strong rule" entailing stronger recharge of the battery.

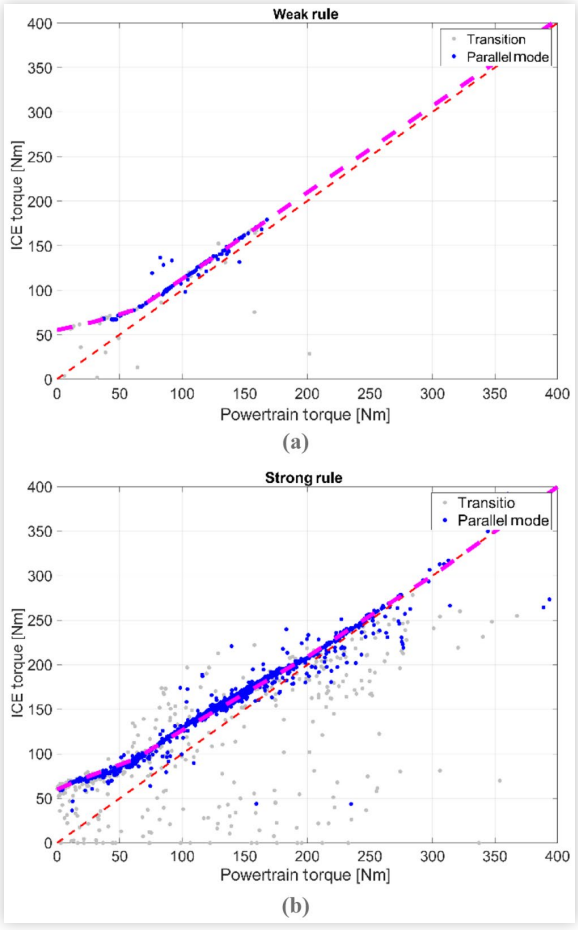

FIGURE 16 WLTC driving cycle—Share of the energy produced by the ICE with respect to its relative load. Green: experimental data; blue: ICE-only mode (obtained through numerical simulation). Engine efficiency vs load trend shown on the right axis.

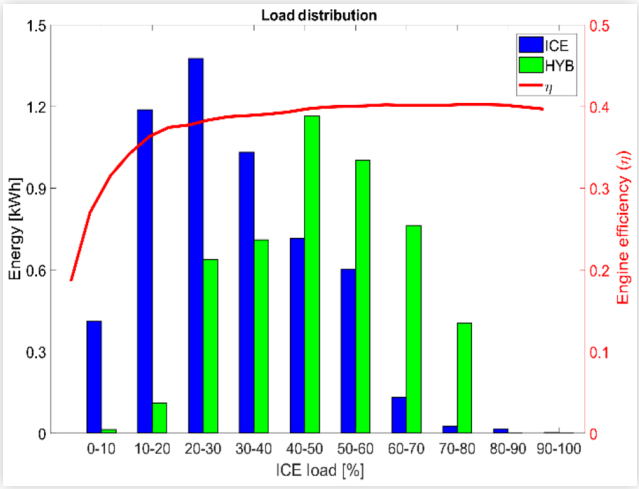

3.3. Flowchart of the Supervisory Controller

All the rules extracted in the previous sections have been summarized in Figure 17. Although the real control strategy could be more complex than the sketch in the figure, the flowchart explains quite well the overall behavior of the supervisory controller. The following notation is used in the flowchart: "Rule_on" and "Rule_off" are the thresholds for switching the engine on and off, respectively, and were shown in Figure 11; SoC_{min1} is the minimum SoC that can be reached in CD operation; it is equal to 0.13 and has been extracted from Table 3; SoC_t corresponds to the max SoC value for CS operations (i.e., the system exits from CS operation as soon as the SoC reaches SoC_t), and it is equal to 0.20. In summary, if the battery SoC is sufficiently high, the EMS makes the vehicle operate in EV mode (i.e., only the EM provides the required power). If the power request exceeds the max performance of the EM, the ICE is switched on, and the vehicle is propelled in parallel mode (both the ICE and the EM concur to provide the requested power), until the rule governing the ICE switching off is not triggered. When the battery SoC reaches the SoC_{min1}, the strategy followed by the EMS changes, and the new rules are aimed at guaranteeing the charge sustainability. In CS operation, the vehicle is propelled from a standstill by the EM, but then the ICE is switched on according to the law shown in Figure 11(a). The ICE switching off rule does not differ too much from the one governing the CD phase and was illustrated in Figure 11(b). Finally, through the combination of an LPM strategy—illustrated in Figure 14—and an additional condition inhibiting the ICE switching on above a certain SoC threshold (SoC_t), the charge sustainability is guaranteed.

3.4. GPS Information Dependency

According to the car manufacturer, the vehicle EMS employs an intelligent operating strategy that takes into account the navigation data, topography, speed limits, and traffic conditions of the entire planned route so that the electric driving mode can be activated when it is most appropriate for the route [32]. In order to highlight any change in the EMS rules depending on the GPS information, a special analysis was carried out. The instrumented vehicle travelled twice the same route: during the first run (RDE_1), the navigation system was disabled, while in the second one (RDE_2) it was enabled. The characteristic values of both cycles were summarized in Table 2, while their vehicle speed profiles are depicted in Figure 18: the small differences between the two profiles can be mainly linked to the variability of real driving conditions (e.g., road, traffic, etc.).

Figure 19(a) and (b) represent the RDE_1 (navigation system switched off), while Figure 19(c) and (d) represent the RDE_2 (navigation system switched on). In the RDE_1, as detailed in Figure 19(a) and (b), more than 40 km are covered in the CD phase, leading to an almost linear SoC depletion with distance. The only sections in which the SoC is not further decreased correspond to the intervals in which the ICE is switched on and the EM is simply motored. On the contrary, as demonstrated by Figure 19(c) and (d), when the vehicle mission is communicated by the driver through the navigation device, the EMS changes its decisions ensuring that the last stage of the journey (the urban one) can be covered in all-electric mode. As illustrated in Figure 19(d), although the test is started with a fully charged battery, the highway section is performed in parallel mode and the battery SoC

FIGURE 17 Flowchart of the supervisory controller extracted from experimental data.

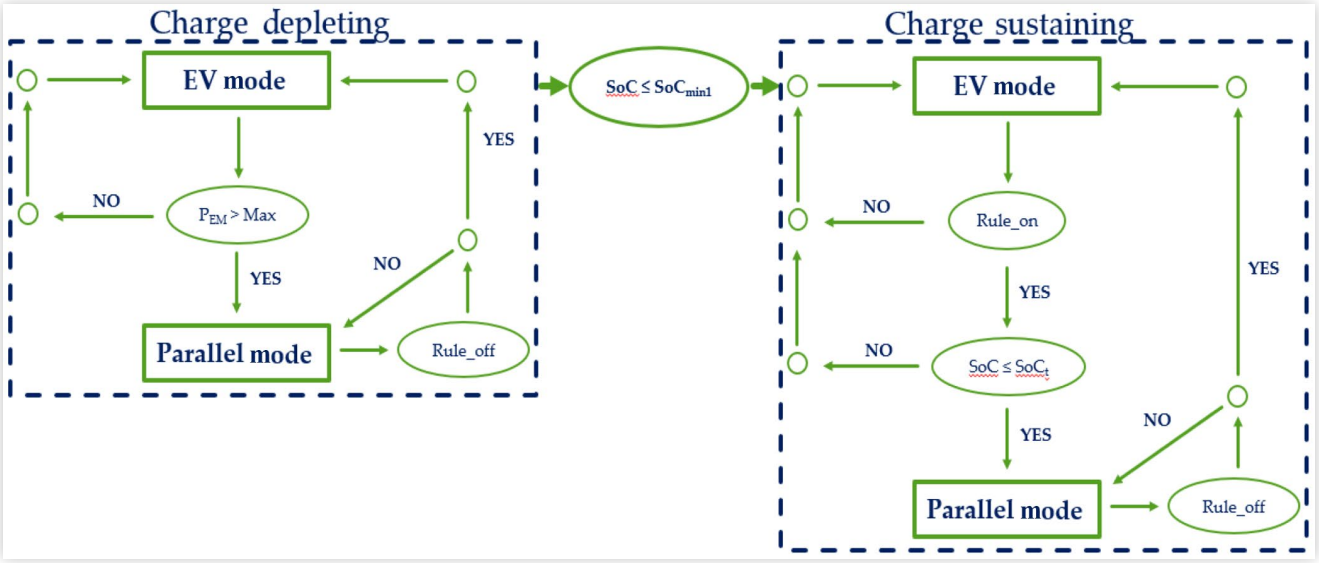

FIGURE 18 Vehicle speed profile of the instrumented vehicle travelling twice the same route: RDE_1 and RDE_2 with the navigation system disabled and enabled, respectively.

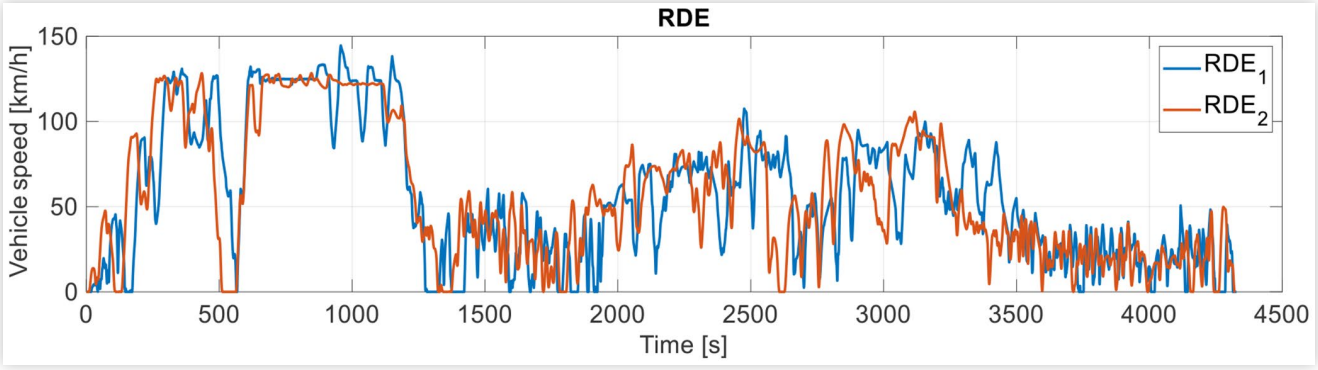

remains almost constant. Then, when the urban section begins, the EV mode is mainly used for propelling the vehicle, and the battery SoC is linearly depleted, but the battery is not fully discharged at the end of the test.

To highlight the different behavior adopted by the EMS when the navigation system was switched on, Figure 20 displays the operating modes, along with the power delivered by the ICE and the EM, only for the highway section. As evident from Figure 20(b) and (c), when the navigation system is switched off, the ICE is started only when the power requested by the driver exceeds the max performance of the EM. On the contrary, as illustrated in Figure 20(e) and (f), when the navigation system is switched on, the electric power source propels the vehicle only during low speed and acceleration phases. When the ICE is switched on, the vehicle is propelled in ICE-only mode, as it can be observed between 650 s and 1100 s, where the power delivered by the EM is null.

The power split chosen by the intelligent operating strategy can be more deeply understood from Figure 21, where all the EM operating points during the RDE_2 are plotted. It can be observed that, apart from the transitional phases, when the ICE is switched on, it provides all the required power, and the EM is simply motored. These findings suggest that the availability of GPS information does not deeply change the rules explained in Figure 17. In fact, without the navigation system, when the ICE is switched on in the CD phase, the vehicle is propelled in the ICE-only mode. In Figure 22, the rule governing the ICE switching on during the RDE_2 is compared to the one obtained during the WLTC in the CS phase. As evident from the figure, the identified pattern recalls

FIGURE 19 Intelligent drive management depending on the vehicle mission profile: RDE_1 (on the left) and RDE_2 (on the right) with the navigation system disabled and enabled, respectively.

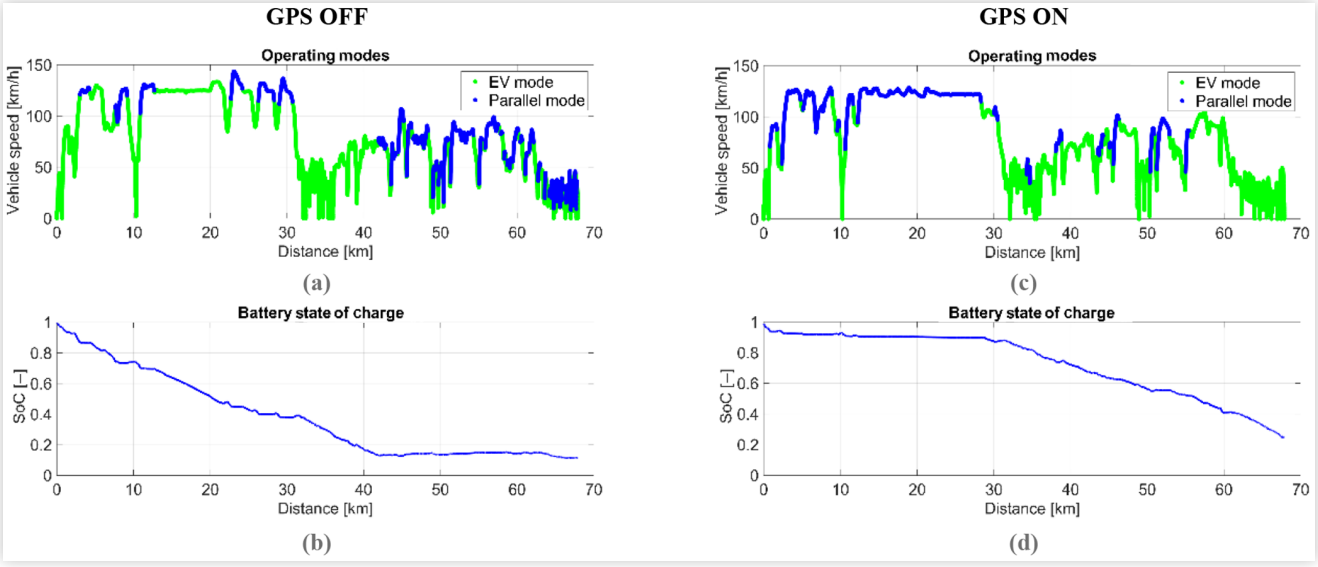

FIGURE 20 Power split during the highway section: RDE_1 (on the left) and RDE_2 (on the right) with the navigation system disabled and enabled, respectively.

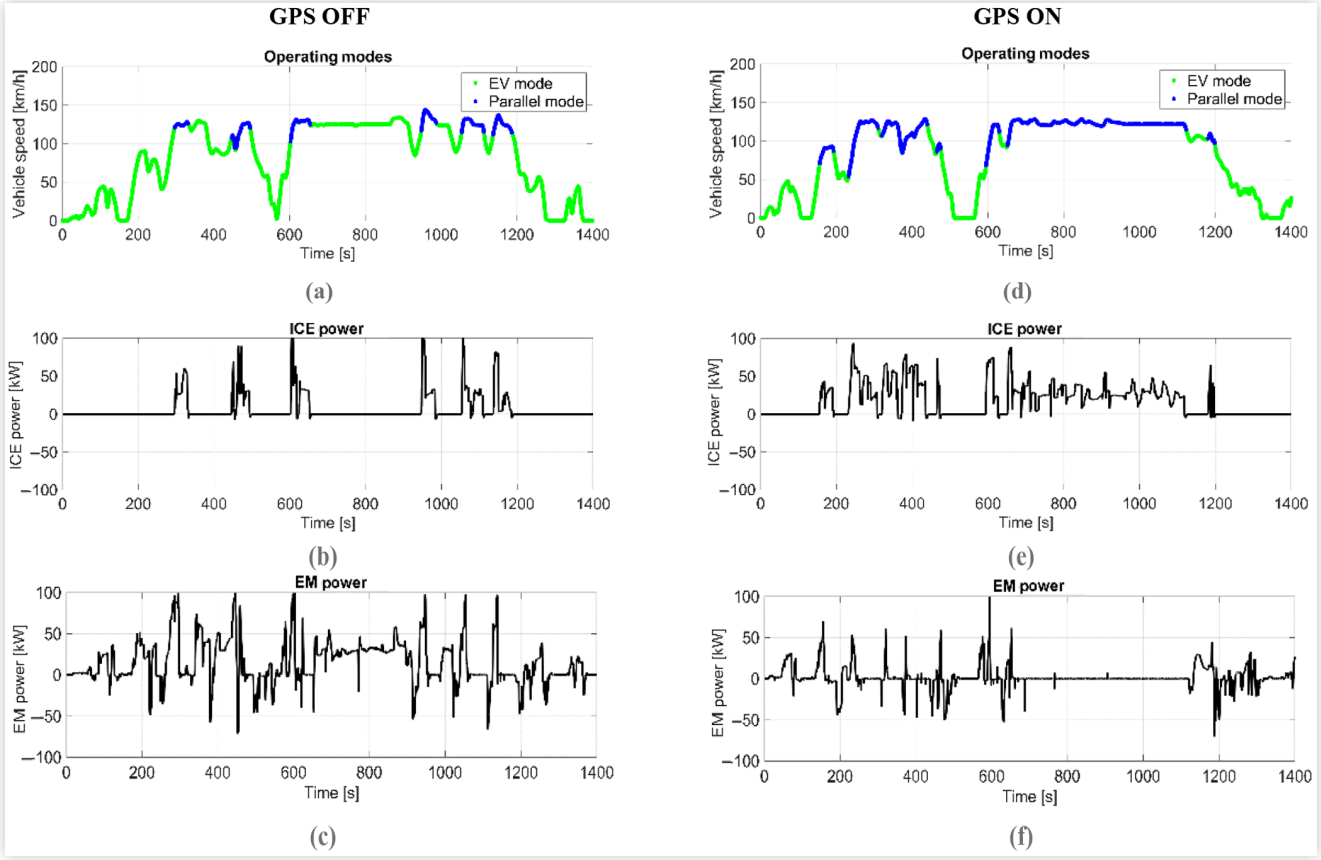

FIGURE 21 RDE_2—EM power represented in the function of the total powertrain power. Green dots: EV mode; blue dots: parallel mode; gray dots: transition phases, i.e., the engine status and the clutch engagement are changing.

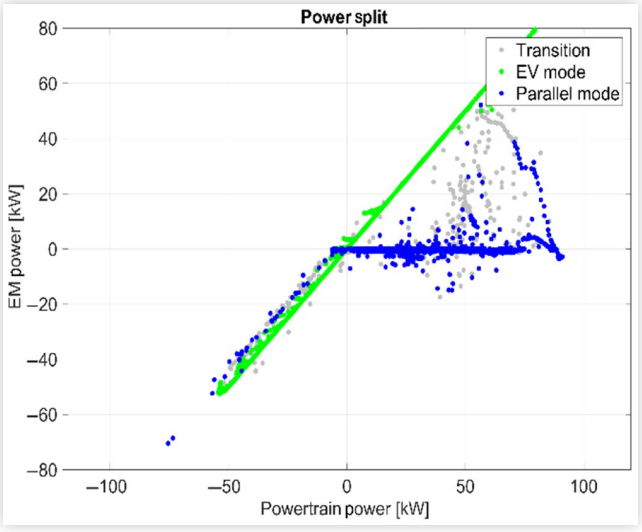

FIGURE 22 Mapping of engine switching on during the RDE_2 and the WLTC: engine ignition points as a function of vehicle acceleration and speed.

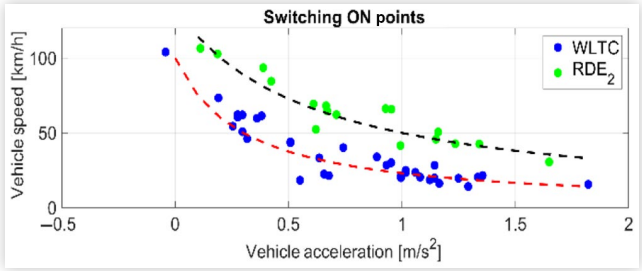

the one explained in Figure 11 but shifted toward higher speeds and accelerations.

3.5. Virtual Test Rig: EMS Modelling

The procedure described in the previous sections was carried out on a huge number of driving cycles to obtain a set of comprehensive rules valid in a wide range of driving conditions. Then a virtual test rig of the tested vehicle, developed in the GT-SUITE environment, was used to validate the set of extracted rules against the experimental data. In this context, aimed at estimating the fuel consumption, a quasi-static approach was adopted [33]: a vehicle driver—i.e., a Proportional-Integral-Derivative (PID) controller—compares the actual vehicle speed to a target one and generates a power demand profile to follow the target speed. The code computes the actual vehicle speed by solving the longitudinal vehicle dynamics, while fuel consumption and pollutant emissions are calculated based on steady-state performance maps, experimentally measured. The powertrain parameters used in the vehicle model were derived from [28] and are shown in Table 1. As far as the EMS is concerned, it was fully developed in a Simulink® environment. The ICE switching on and off is governed by the rules presented in the previous section, while a weighted average of the two LPM laws, based on the instantaneous battery SoC, is implemented to introduce a smooth transition between strong and weak conditions (see Figure 23).

In order to properly estimate the energy recovered through regenerative braking and consequently replicate the experimental SoC trajectory, it is of paramount importance to capture the powertrain contribution to the vehicle braking system. In a hybrid vehicle, during braking maneuvers, the regenerative braking depends also on comfort and safety levels and on the battery current limits. Indeed, particular attention should be paid to vehicle dynamics in an RWD configuration, such as the case study, where the EM contributes to the rear axle braking. In the current work the vehicle braking system is managed through experimental maps, obtained by DiPierro et al. in [28], where the braking power ratio—i.e., powertrain regenerative braking over total braking power—is expressed as a function of vehicle speed and acceleration.

It is worth mentioning that the battery characterization and the reverse engineering were conducted with an SoC variable acquired from the CAN network, representing the dashboard displayed value. Hence, the SoC provided by the battery model matches the dashboard value in the range of 0-100% and is an indication of the actual energy capacity available to the user. Moreover, it should also be pointed out that, during the experimental campaign, it was not possible to perform a detailed characterization of the HV battery chemistry. Therefore, the HV battery was modelled according to data available in the scientific literature [34, 35]: its parameters (e.g., cell internal resistances, cell open-circuit voltage, etc.) were calibrated to obtain a correct matching of the experimental reference SoC.

It should, finally, be noted that the model simulation was aimed at reproducing the vehicle behavior in standard driving. Some particular conditions entailing variations in the rules followed by the EMS were not taken into account in the simulations, e.g., the missions where the driver communicates the vehicle route to the EMS through the GPS navigation system; the type-approval procedure featuring a cold engine (i.e., the cycle performed one day after Condition A).

FIGURE 23 2D function of the LPM law, based on the total torque required by the driver and the instantaneous battery SoC.

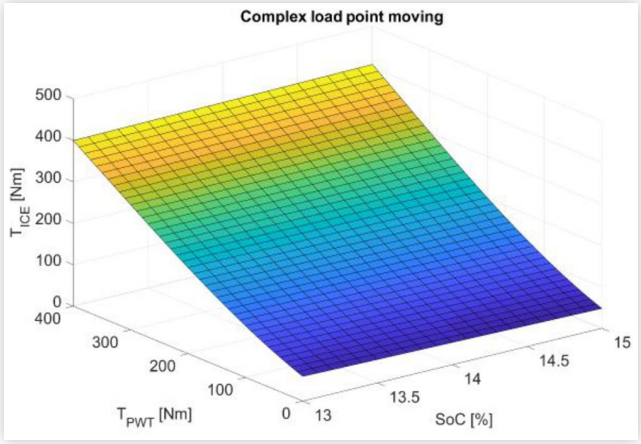

3.6. Model Validation

The model validation was carried out along the regulatory driving cycles, but in line with the approach adopted for the rule extraction, only the results obtained in the WLTC are shown. It was performed both in CD and CS phases. In fact, the CD phase can be considered as a proving ground for assessing the fidelity of the vehicle longitudinal dynamics modelling and of the accuracy of the battery and the EM simulations. Only after the model is able to accurately capture the experimental behavior in the CD phase, it can be tested in the CS phase in order to assess the robustness of the EMS implementation.

In Figure 24 the results derived from numerical simulation (red line) are compared with the experimental measurements (black dashed line) for the first WLTC performed in CD mode. For the sake of clarity, the cycle is subdivided into two sections: both plots (a) and (d) illustrate the vehicle speed profile. Although it is a dynamic one (the speed is not imposed but it is seen as a target), the model is able to excellently match the experimental vehicle speed, even for the more aggressive speed variations. As evident from plots (b) and (e), the torque delivered by the EM is well captured over the entire cycle. As a result, as shown in (c) and (f), the battery SoC prediction coming from the simulation is highly reliable.

Both NEDC and WLTC results (summarized in Table 4) confirmed the accuracy of the model in terms of vehicle longitudinal dynamics and balance of the electrical board net.

FIGURE 24 Comparison between numerical simulation (red line) and experimental measurements (black dashed line) for the WLTC performed in the CD phase. (a), (d) Vehicle speed; (b), (e) EM torque; (c), (f) Battery SoC.

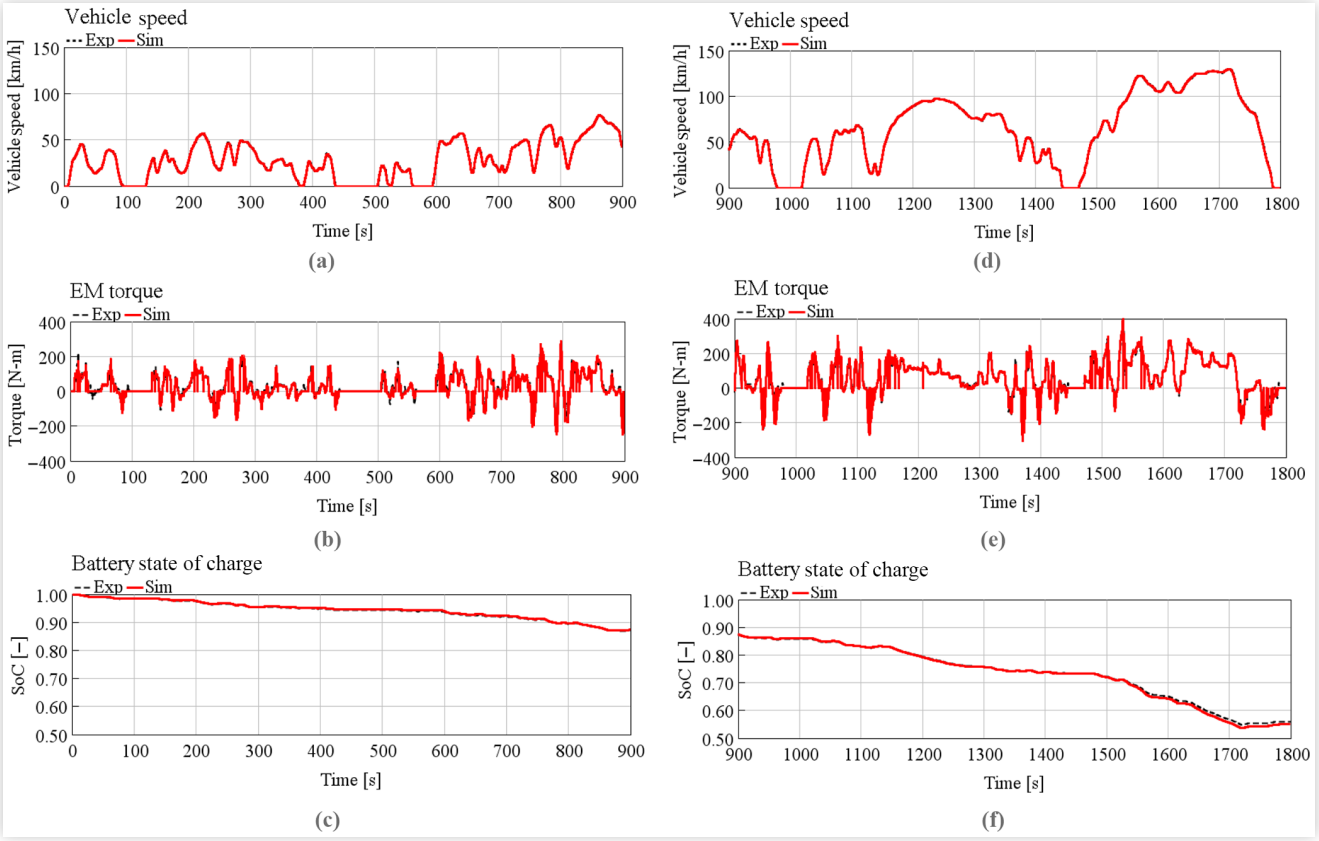

Figure 25 shows the comparison between experimental data and numerical simulation results for the WLTC performed in CS mode. Compared to Figure 24, the following ICE variables have been added: speed, torque, and fuel rate. As illustrated by plots (b) and (h)—all the plots on the right represent an enlargement of the dashed area on the left—the EM torque matching between simulation and experimental is more than satisfying. As evident from plots (d) and (j), the ICE rotational speed is well captured over the entire cycle, and apart from some occasional cases, the model correctly predicts the ICE on and off events. Thus the model accurately reproduces the ICE torque and fuel rate.

The results coming from the WLTC, along with the ones obtained in the NEDC, are shown in Table 5. Both the final SoC and the fuel economy obtained in the simulation are quite compelling.

TABLE 4 Comparison between experimental data and simulation results for the regulatory driving cycles in the CD phase.

	Final SoC [—]	
Cycle	Experimental	Simulation
NEDC	0.82	0.82 (+0.7%)
WLTC	0.56	0.55 (–1.8%)

4. Results and Discussion

In this section, the model is tested over the RDE_3 cycle to prove its capabilities to predict the vehicle behavior in a real-driving scenario. It should be noted that, in order to perform a robust validation, this cycle was not included in the EMS rules extraction. In Figure 26 the results coming from the numerical simulation are compared with the experimental measurements. Plots (d) and (j) demonstrate that, similar to the WLTC, the ICE rotational speed is well captured over the entire cycle, and apart from some occasional cases, the model correctly predicts the ICE on and off events. Moreover, as evident from (c), the instant of transition from CD to CS mode is well captured. Even though the cycle is highly transient, the EM and ICE operating points are correctly reproduced in terms of speed and load. As a result, the battery SoC profile—plots (c) and (i)—shows a remarkable agreement with the measured data: for the majority of the trip, the difference between measurement and simulation lays within the ±5% limit.

FIGURE 25 Comparison between numerical simulation (red line) and experimental measurements (black dashed line) for the WLTC performed in the CS phase. (a), (g) Vehicle speed; (b), (h) EM torque; (c), (i) Battery SoC; (d), (j) ICE speed; (e), (k) ICE torque; (f), (l) Fuel rate. Plots on the right represent an enlargement of the dashed area on the left.

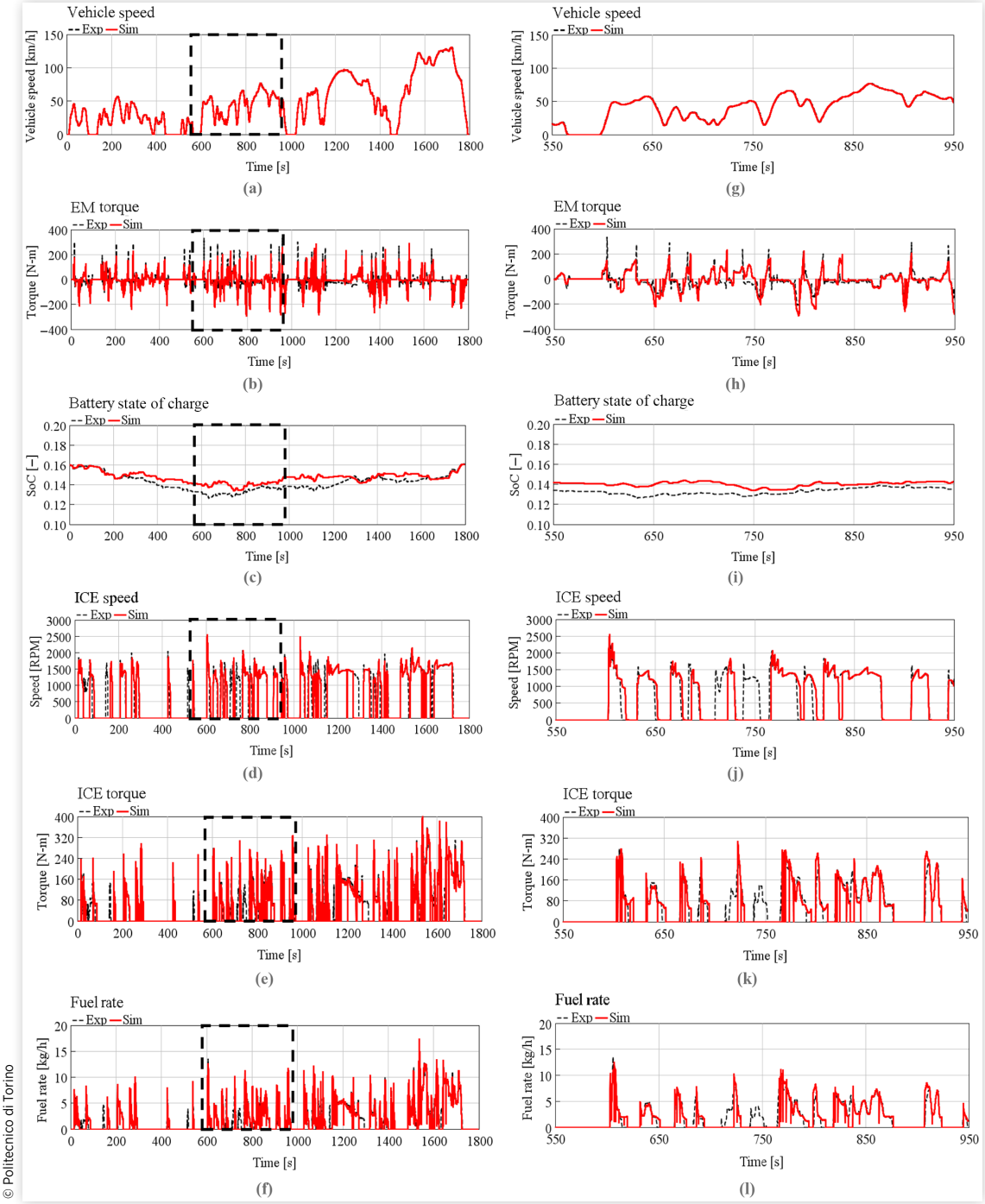

TABLE 5 Comparison between experimental data and simulation results for the regulatory driving cycles in the CS phase.

	CO_2 specific emissions [g/km]		Final SoC [—]	
Cycle	Experimental	Simulation	Experimental	Simulation
NEDC	131	128 (−2.3%)	0.15	0.15 (−0.3%)
WLTC	142	139 (−2.1%)	0.16	0.16 (−0.2%)

FIGURE 26 Comparison between numerical simulation (red line) and experimental measurements (black dashed line) for the RDE_3. (a), (g) Vehicle speed; (b), (h) EM torque; (c), (i) Battery SoC; (d), (j) ICE speed; (e), (k) ICE torque; (f), (l) Fuel rate. Plots on the right represent an enlargement of the dashed area on the left.

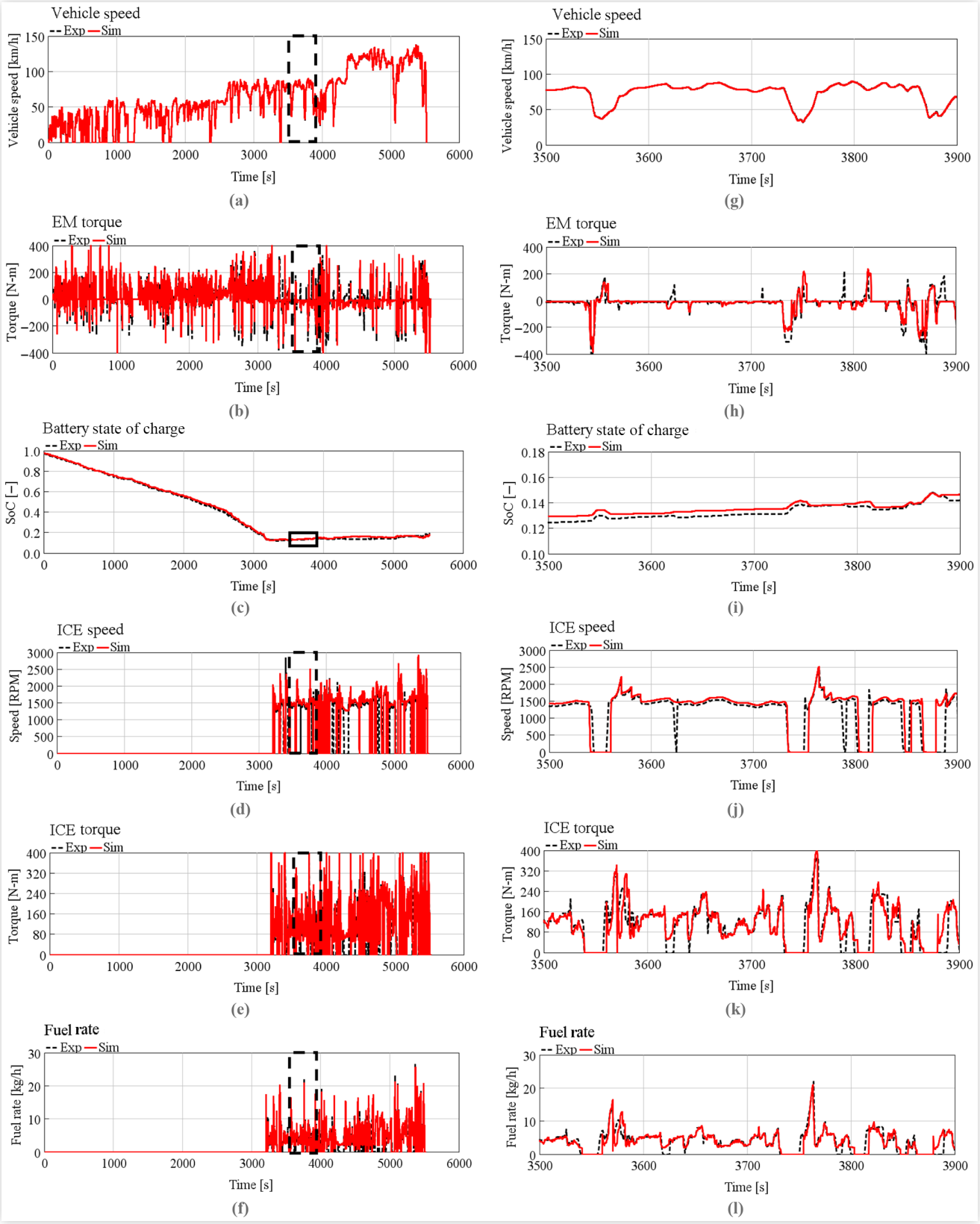

TABLE 6 Comparison between experimental data and simulation results for RDE_3.

	CO_2-specific emissions [g/km]		Final SoC [—]	
Cycle	Experimental	Simulation	Experimental	Simulation
RDE_3	95	96 (+1.0%)	0.19	0.18 (−4.7%)

The accuracy of the model in terms of fuel economy and final SoC prediction can be confirmed by the results shown in Table 6. The compelling agreement between experimental data and numerical results leads to errors, over the entire test, of 4.7% and 1.0% on the estimation of the final SoC and the CO_2 specific emissions, respectively. Although the discrepancy in terms of final SoC may appear quite significant (4.7%), it is instead quite limited if compared with the energy required during the entire driving cycle, i.e., less than 0.1 kWh over a total energy request of 21.6 kWh, which corresponds to 0.44%.

Since the model simulation correctly reproduces the SoC trajectory and the CO_2 specific emissions also in the case of real driving conditions, it seems that the energy management strategy based on the extracted rules is well designed to mimic the real performance of the vehicle. These results lead to confirm the robustness of the presented methodology for reverse engineering the strategy implemented in the EMS of a real vehicle.

5. Conclusions and Future Work

In this article, a generalized methodology for extracting the strategy implemented in the EMS of a commercially available vehicle was presented. A Euro 6d-temp P2 diesel vehicle was considered as a test case. The study relied on a huge amount of experimental data collected in a wide range of driving conditions. The proposed approach described how to handle the acquired data in order to extract the control rules followed by the hybrid powertrain and to point out the dependency of the EMS decisions on the powertrain's main operating variables. The procedure was carefully described using the WLTC as a test case. Then a virtual test rig of the tested vehicle was built and used for the validation of the set of extracted rules against the experimental data. Comparison between measurement and simulation results showed a good agreement, with a deviation of the CO_2 specific emissions being of about 1-2%. The error in the final battery SoC estimation is less than 0.5% on the TA procedures, and less than 5% on the RDE cycle.

The purpose of this article was to provide some practical guidelines for extracting the strategy adopted by the EMS of a (P)HEV without having any direct access to it. The acceptable accuracy of the vehicle model in predicting the SoC trajectory and the fuel consumption proved the robustness of the proposed methodology. In order to achieve these results, the following points were of paramount importance in the experimental activity:

1. Testing the vehicle both on the chassis dynamometer and on the road in real-world scenarios;
2. Testing the dependency of the EMS on the GPS information by travelling the same route with the navigation system alternatively switched on and off;
3. Performing the characterization of the powertrain without an expensive teardown (only the ICE needs a detailed experimental investigation in order to obtain the fuel consumption maps).

By carefully following these premises, the proposed methodology could be applied for the experimental investigation of a generic (P)HEV in order to identify the main rules followed by its powertrain control logic.

Finally, future works will use the validated virtual test rig to assess the fuel economy potential of more sophisticated energy management strategies: in fact, thanks to the introduction of look-ahead technologies, such as V2X connectivity, it could be possible to obtain a reliable speed forecasting and exploit this information in the energy management of HEVs. As an example, Figure 27 shows a synoptic diagram of a technique developed in [36]: a neural network is used for choosing the equivalence factor of the well-known ECMS formulation depending on the forecasted vehicle speed.

FIGURE 27 Enhancement of the fuel economy potential of the investigated vehicle: exploiting information coming from V2X connectivity in the energy management problem.

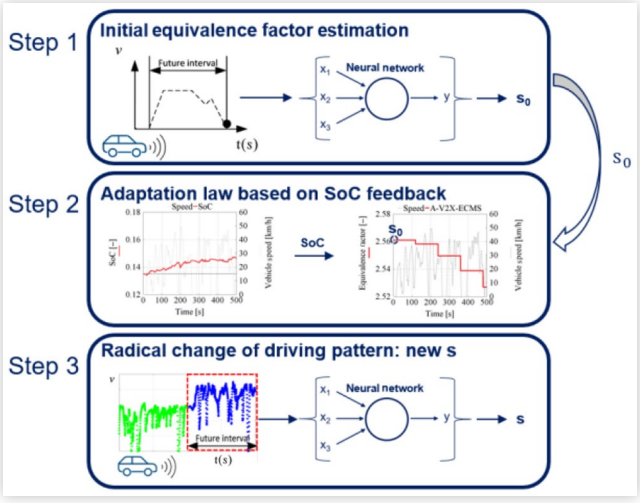

Acknowledgments

This research was financially supported by Regione Piemonte (Italy) under the Program L.R. 34/04–Programma d'intervento per le attività produttive 2011/2017–Asse 3 (Internazionalizzazione), Misura 3.1 "Contratto d'insediamento". Progetto: "Sviluppo di una nuova generazione di sistemi di propulsione di veicoli ibridi ed elettrici"/"Development of a new generation of hybrid and electric propulsion systems", -Soc. FEV Italia Srl e Politecnico di Torino.

Contact Information

Luciano Rolando
Energy Department
Politecnico di Torino
c.so Duca degli Abruzzi, 24
10129 Torino - ITALY
luciano.rolando@polito.it

Definitions/Abbreviations

AT - Automatic Transmission
AWD - All-Wheel Drive
BMEP - Brake Mean Effective Pressure
BMS - Battery Management System
BSFC - Brake-Specific Fuel Consumption
CAN - Controller Area Network
CD - Charge Depleting
COP21 - 2015 United Nations Climate Change Conference
CO_2 - Carbon Dioxide Emissions
CS - Charge Sustaining
DC - Direct Current
ECMS - Equivalent Consumption Minimization Strategy
ECU - Electronic Control Unit
EM - Electric Machine
EMS - Energy Management System
EV - Electric Vehicle
GPS - Global Positioning System
GHG - Greenhouse Gas
HCU - Hybrid Control Unit
HPCU - Hybrid Power Control Unit
HEV - Hybrid Electric Vehicle
HV - High Voltage
ICE - Internal Combustion Engine
Li-NMC - Li-Ion Nickel-Manganese-Cobalt-oxide
LPM - Load Point Moving
LV - Low Voltage
NEDC - New European Driving Cycle
NMC - Nickel-Manganese-Cobalt
OBD - OnBoard Diagnostic
PEMS - Portable Emissions Measurement System
PHEV - Plug-in Hybrid Electric Vehicle
PID - Proportional-Integral-Derivative
PM - Permanent Magnet
RDE - Real Driving Emission
RWD - Rear Wheel Drive
SoC - State of Charge
TA - Type Approval
TC - Torque Converter
V2I - Vehicle-to-Infrastructure
V2X - Vehicle-to-Everything
WLTC - Worldwide Harmonized Light-duty Cycle

References

1. Lindsey, R., "Climate Change: Atmospheric Carbon Dioxide," accessed October 2020, https://www.climate.gov/news-features/understanding-climate/climate-change-atmospheric-carbon-dioxide.
2. Lindsey, R., "Climate and Earth's Energy Budget," accessed October 2020, https://earthobservatory.nasa.gov/features/EnergyBalance.
3. European Commission, "Paris Agreement," accessed November 2020, http://ec.europa.eu/clima/policies/international/negotiations/paris_en.
4. European Parliament, "CO_2 Emissions from Cars: Facts and Figures," accessed November 2020, http://www.europarl.europa.eu/news/en/headlines/society/20190313STO31218/co2-emissions-from-cars-facts-and-figures-infographics.
5. European Environment Agency, "Greenhouse Gas Emissions from Transport," accessed November 2020, https://www.eea.europa.eu/data-and-maps/indicators/transport-emissions-of-greenhouse-gases/transport-emissions-of-greenhouse-gases-12.
6. Mock, P. "The Role of Standards in Reducing CO_2 Emissions of Passenger Cars in the EU," ICCT Briefing Paper, accessed November 2020, https://www.theicct.org/sites/default/files/publications/Role_of_EU-CO2_Standard_20180212.pdf.
7. European Commission, "CO_2 Emission Performance Standards for Cars and Vans (2020 Onwards)," accessed November 2020, https://ec.europa.eu/clima/policies/transport/vehicles/regulation_en.
8. ICCT, "European Vehicle Market Statistics—Pocketbook 2018/19," 64, 2018.

9. Millo, F., Rolando, L., Fuso, R., and Mallamo, F., "Real CO_2 Emissions Benefits and End User's Operating Costs of a Plug-In Hybrid Electric Vehicle," *Applied Energy* 114 (2014): 563-571, https://doi.org/10.1016/j.apenergy.2013.09.014.
10. Sciarretta, A. and Guzzella, L., "Control of Hybrid Electric Vehicles," *IEEE Control Systems Magazine* 27, no. 2 (2007): 60-70, https://doi.org/10.1109/MCS.2007.338280.
11. Salmasi, F.R., "Control Strategies for Hybrid Electric Vehicles: Evolution, Classification, Comparison, and Future Trends," *IEEE Transactions on Vehicular Technology* 56, no. 5 (2007): 2393-2404, https://doi.org/10.1109/TVT.2007.899933.
12. Onori, S., Serrao, L., and Rizzoni, G., *Hybrid Electric Vehicles: Energy Management Strategies* (London: Springer, 2016), ISBN:978-1-4471-6781-5.
13. Rolando, L. "An Innovative Methodology for the Development of HEVs Energy Management Systems," PhD thesis, Politecnico di Torino, 2012, ISBN:978-3639514513.
14. Tran, D.D., Vafaeipour, M., El Baghdadi, M., Barrero, R. et al., "Thorough State-of-the-Art Analysis of Electric and Hybrid Vehicle Powertrains: Topologies and Integrated Energy Management Strategies," *Renewable and Sustainable Energy Reviews* 119 (2019): 109596, https://doi.org/10.1016/j.rser.2019.109596.
15. Ali, A.M. and Söffker, D., "Towards Optimal Power Management of Hybrid Electric Vehicles in Real-Time: A Review on Methods, Challenges, and State-of-the-Art Solutions," *Energies* 11 (2018): 476, https://doi.org/10.3390/en11030476.
16. Bertsekas, D., *Dynamic Programming and Optimal Control* (Belmont, MA: Athena Scientific, 1995), ISBN:1-886529-26-4.
17. Sundström, O., Ambühl, D., and Guzzella, L., "On Implementation of Dynamic Programming for Optimal Control Problems with Final State Constraints," *Oil and Gas Science and Technology - Rev. IFP* 65 (2009): 91-102, https://doi.org/10.2516/ogst/2009020.
18. Paganelli, G. "Conception et commande d'une chaîne de traction pour véhicule hybride parallèle thermique et électrique," PhD thesis, Université de Valenciennes, Valenciennes, 1999.
19. Paganelli, G., Guerra, T.M., Delprat, S., and Santin, J., "Simulation and Assessment of Power Control Strategies for a Parallel Hybrid Car," *Proceedings of the Institution of Mechanical Engineers, Part D: Journal of Automobile Engineering* 214 (2000): 705-717.
20. Serrao, L., Onori, S., and Rizzoni, G., "ECMS as a Realization of Pontryagin's Minimum Principle for HEV Control," *Proceedings of the American Control Conference* (2009): 3964-3969, https://doi.org/10.1109/ACC.2009.5160628.
21. Sabri M., M. F., Danapalasingam K.A., and Rahmat M.F.. "A Review on Hybrid Electric Vehicles Architecture and Energy Management Strategies," *Renewable and Sustainable Energy Reviews* 53:1433-1442, 2016, https://doi.org/10.1016/j.rser.2015.09.036.
22. Van Barel, G., Huybrechts, T., Vanommeslaeghe, Y., Blontrock, D. et al., "Automatic Reverse Engineering of CAN BusData Using Machine Learning Techniques," 2017, https://doi.org/10.1007/978-3-319-69835-9_71.
23. Vinot, E., Scordia, J., Trigui, R., Jeanneret, B. et al., "Model Simulation, Validation and Case Study of the 2004 THS of Toyota Prius," *International Journal of Vehicle Systems Modelling and Testing* 3 (2008): 139-167, https://doi.org/10.1504/IJVSMT.2008.023835.
24. Kim, N., Rousseau, A., and Rask, E., "Autonomie Model Validation with Test Data for 2010 Toyota Prius," SAE Technical Paper 2012-01-1040, 2012, https://doi.org/10.4271/2012-01-1040.
25. Jeong, J., Lee, W., Kim, N., Stutenberg, K. et al., "Control Analysis and Model Validation for BMW i3 Range Extender," SAE Technical Paper 2017-01-1152, 2017, https://doi.org/10.4271/2017-01-1152.
26. Cubito, C., Rolando, L., Millo, F., Ciuffo, B. et al., "Energy Management Analysis under Different Operating Modes for a Euro-6 Plug-In Hybrid Passenger Car," SAE Technical Paper 2017-01-1160, 2017, https://doi.org/10.4271/2017-01-1160.
27. Doulgeris, S., Dimaratos, A., Zacharof, N., Toumasatos, Z. et al., "Real World Fuel Consumption Prediction via a Combined Experimental and Modeling Technique," *Science of the Total Environment* 734 (2020): 139254, https://doi.org/10.1016/j.scitotenv.2020.139254.
28. DiPierro, G., Galvagno, E., Mari, G., Millo, F. et al., "A Reverse-Engineering Method for Powertrain Parameters Characterization Applied to a P2 Plug-In Hybrid Electric Vehicle with Automatic Transmission," SAE Technical Paper 2020-37-0021, 2020, https://doi.org/10.4271/2020-37-0021.
29. UNECE, "UNECE Regulation No. 83—Revision 5. Uniform Provisions Concerning the Approval of Vehicles with Regard to the Emissions of Pollutants according to the Engine Fuel Requirements," Geneva, 2015, https://tinyurl.com/cxmdcdzy.
30. UNECE, "UNECE Global Technical Regulation No. 15 Worldwide Harmonized Light Vehicles Test Procedure," Geneva, 2015, https://tinyurl.com/859eyr6c.
31. European Commission, "Commission Regulation (EU) 2017/1151 of 1 June 2017 of the European Parliament and of the Council on Type-Approval of Motor Vehicles With Respect to Emissions from Light Passenger and Commercial Vehicles (Euro 5 and Euro 6) and on Access to Vehicle Repair and Maintenance Information, Amending Directive 2007/46/EC of the European Parliament and of the Council, Commission Regulation (EC) No. 692/2008 and Commission Regulation (EU) No. 1230/2012 and repealing Commission Regulation (EC) No. 692/2008," 2017, https://tinyurl.com/53ecjp7s.

32. Media.daimler, "Under the Microscope: The Intelligent Operating Strategy: Better Electric Performance," accessed November 2020, https://tinyurl.com/y37zrbn6.

33. Millo, F., Rolando, L., and Andreata, M., "Numerical Simulation for Vehicle Powertrain Development," in Awrejcewicz, J., (Ed.), *Numerical Analysis—Theory and Application* (InTech, 2011), https://doi.org/10.5772/24111.

34. Samad, N.A., Siegel, J.B., and Stefanopoulou, A.G., "Parameterization and Validation of a Distributed Coupled Electro-Thermal Model for Prismatic Cells," in *Proceedings of the ASME 2014 Dynamic Systems and Control Conference, DSCC 2014*, San Antonio, Texas, USA, 2, 2014, 10.1115/DSCC2014-6321.

35. Samad, N.A., Kim, Y., Siegel, J.B., and Stefanopoulou, A.G., "Influence of Battery Downsizing and SOC Operating Window on Battery Pack Performance in a Hybrid Electric Vehicle," in *2015 IEEE Vehicle Power Propulsion Conference VPPC 2015—Proceedings*, Montreal, Quebec, Canada, 2015, https://doi.org/10.1109/VPPC.2015.7352966.

36. Pulvirenti, L., Rolando, L., and Millo, F., "Energy Management System Optimization Based on V2X Connectivity," in *2021 FISITA World Congress Proceedings*, 2021, Prague, in press, https://doi.org/10.46720/F2020-ADM-087.